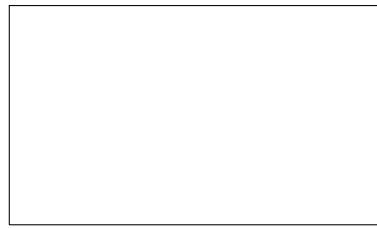


Graphical Abstract

MAAT: Mamba Adaptive Anomaly Transformer with association discrepancy for time series

Abdellah Zakaria Sellam, Ilyes Benaissa, Abdelmalik Taleb-Ahmed, Luigi Patrono, Cosimo Distante



Highlights

MAAT: Mamba Adaptive Anomaly Transformer with association discrepancy for time series

Abdellah Zakaria Sellam, Ilyes Benaissa, Abdelmalik Taleb-Ahmed, Luigi Patrono, Cosimo Distante

- The Mamba Adaptive Anomaly Transformer (MAAT) introduces a Sparse Attention mechanism and integrates the Mamba-Selective State Space Model (Mamba-SSM), enabling it to effectively capture both short-term and long-term temporal dependencies in time series data
- MAAT outperforms existing models like the Anomaly Transformer and DCdetector by achieving higher Accuracy, precision, recall, and F1-scores across benchmark datasets.

MAAT: Mamba Adaptive Anomaly Transformer with association discrepancy for time series

Abdellah Zakaria Sellam^{a,c}, Ilyes Benaissa^a, Abdelmalik Taleb-Ahmed^b,
Luigi Patrono^{a,c}, Cosimo Distante^{a,c}

^a*Department of Innovation Engineering; University of Salento, via
Monteroni, Lecce, 73100, Italy*

^b*Institute d'Electronique de Microelectronique et de Nanotechnologie (IEMN); UMR
8520; Universite Polytechnique Hauts de France; Universite de Lille;
CNRS, , Valenciennes, 59313, France*

^c*Institute of Applied Sciences and Intelligent Systems - CNR, via
Monteroni, Lecce, 73100, Italy*

Abstract

Anomaly detection in time series poses a critical challenge in industrial monitoring, environmental sensing, and infrastructure reliability, where accurately distinguishing anomalies from complex temporal patterns remains an open problem. While existing methods, such as the Anomaly Transformer leveraging multi-layer association discrepancy between prior and series distributions and DCdetector employing dual-attention contrastive learning, have advanced the field, critical limitations persist. These include sensitivity to short-term context windows, computational inefficiency, and degraded performance under noisy and non-stationary real-world conditions. To address these challenges, we present MAAT (Mamba Adaptive Anomaly Transformer), an enhanced architecture that refines association discrepancy modeling and reconstruction quality for more robust anomaly detection. Our work introduces two key contributions to the existing Anomaly transformer architecture: Sparse Attention, which computes association discrepancy more efficiently by selectively focusing on the most relevant time steps. This reduces computational redundancy while effectively capturing long-range dependencies critical for discerning subtle anomalies. Additionally, a Mamba-Selective State Space Model (Mamba-SSM) is integrated into the reconstruction module. A skip connection bridges the original reconstruction and the Mamba-SSM output, while a Gated Attention mechanism adaptively fuses features from both pathways. This design dynamically balances fidelity and con-

textual enhancement, improving anomaly localization and overall detection performance.

Extensive experiments on benchmark datasets demonstrate that MAAT significantly outperforms prior methods, achieving superior anomaly distinguishability and generalization across diverse time series applications. By addressing the limitations of existing approaches, MAAT sets a new standard for unsupervised time series anomaly detection in real-world scenarios.

Keywords: MAAT, Transformer, Association Discrepancy, Gated Attention, Mamba-SSM, Sparse Attention, Anomaly Detection, Unsupervised Learning

1. Introduction

Anomaly detection in time series data is crucial across various domains, including finance, healthcare, industrial monitoring, and cybersecurity. Identifying unexpected or abnormal events in sequential data is essential for preventing system failures, detecting fraudulent activities, and ensuring operational efficiency. Traditionally, this task has been addressed using statistical methods, such as ARIMA [1] and Gaussian Processes [2], which rely on the assumption that anomalies can be identified as deviations from predicted values. However, these methods often struggle with real-world time series data complex, high-dimensional nature, especially when the underlying patterns are non-linear or when the anomalies are subtle [3].

With the advent of machine learning, more sophisticated models have been developed to address these challenges. Techniques such as Support Vector Machines (SVMs)[4], Random Forests[5], and Hidden Markov Models (HMMs)[6] were among the first machine learning methods applied to anomaly detection in time series. These models improved traditional statistical methods by learning from data rather than relying solely on predefined rules. However, they still required significant manual feature engineering and often did not fully capture the temporal dependencies inherent in sequential data.

The introduction of deep learning models marked a significant shift in time series anomaly detection. Recurrent Neural Networks (RNNs)[7], and Long Short-Term Memory (LSTM)[8] networks, in particular, have become popular due to their ability to model long-term dependencies in time series data. These models can learn complex temporal patterns directly from the

data, making them well-suited for tasks such as anomaly detection, where subtle deviations from the norm need to be identified [6]. Additionally, the use of autoencoders and their variants, such as Variational Autoencoders (VAEs)[9] and Adversarial Autoencoders[10], has further advanced the field by enabling unsupervised anomaly detection through the reconstruction of standard data patterns [11].

Reconstruction-based methods are widely adopted in time series anomaly detection because they can model standard data patterns and identify deviations as anomalies. These methods typically involve training neural networks, such as autoencoders[8], to reconstruct input data, assuming that standard data can be accurately reconstructed while anomalies yield higher reconstruction errors. Autoencoders have been extensively used for this purpose because of their capacity to learn compressed representations and effectively reconstruct signals [12]. Similarly, recurrent neural networks (RNNs) and long short-term memory (LSTM) networks have been employed to capture temporal dependencies in sequential data during reconstruction tasks [8]. However, one limitation of these methods is their reliance on reconstruction loss as the sole anomaly detection criterion. This may lead to false positives when specific anomalous points exhibit patterns similar to standard data. To address this issue, The application of Transformer architectures to time series data has opened new possibilities. Transformers[13], initially developed for natural language processing, use a self-attention mechanism that allows them to model complex dependencies over long sequences. This capability is particularly advantageous for time series anomaly detection, where capturing local and global temporal patterns is crucial. In addition to the standard self-attention mechanism, various adaptations have been proposed to enhance the modeling of time series data. Gated attention mechanisms[14], for instance, integrate gating structures to dynamically control the flow of information, enabling the model to focus on relevant temporal features and improve performance in time series forecasting tasks. Sparse attention[15] mechanisms have also been introduced to improve the efficiency of Transformers when handling long sequences. By limiting the attention computation to a subset of the input sequence, sparse attention reduces computational complexity while maintaining the ability to capture essential dependencies. This approach is particularly beneficial for long-sequence time-series forecasting, where traditional attention mechanisms may become computationally prohibitive.

Recent advancements in time series anomaly detection have led to sophisticated approaches like the Anomaly Transformer [16], which leverage

association discrepancy learning to distinguish normal from abnormal points without solely relying on reconstruction loss. This innovative framework employs a Gaussian kernel and attention mechanisms to model both prior-association and series-association discrepancies, comparing the expected and observed temporal associations to set a new standard in Accuracy and robustness. It addresses long-standing computational efficiency and scalability challenges that have traditionally affected reconstruction-based methods, particularly in high-dimensional or multivariate datasets. This evolution from simple statistical models to advanced deep learning architectures underscores the growing complexity and critical importance of detecting anomalies that may signal crucial events or failures. It highlights the need for models capable of pushing the boundaries of anomaly detection in increasingly complex data environments. This approach achieves state-of-the-art performance by amplifying the distinguishability between normal and abnormal data points through a minimax strategy. However, despite its advancements, the Anomaly Transformer faces several limitations. Reliance on self-attention mechanisms restricts its ability to model long-range dependencies in small window sizes, and noise and non-stationary patterns can distort association discrepancy metrics, increasing false positives during transient but normal system fluctuations. Although more efficient than traditional reconstruction-based methods.

Furthermore, DCdetector [17] simplifies the anomaly detection process by employing a dual-attention contrastive structure that eliminates the need for complex components like Gaussian kernels or reconstruction losses. Instead, it relies on contrastive learning to enhance the separation between anomalies and standard points. This approach introduces a purely contrastive learning framework for time series anomaly detection, avoiding reconstruction-based methods that often struggle with anomalies and encoder-decoder design challenges. DCdetector utilizes a dual-channel architecture, comprising patch-wise and in-patch branches, to capture both global and local temporal dependencies, ensuring robust representations for expected points while highlighting discrepancies in anomalous ones. Its channel independence patching mechanism efficiently processes multivariate time series inputs, reducing parameter complexity and mitigating overfitting risks. The model training relies on a contrastive loss function based on Kullback-Leibler divergence, which maximizes representation consistency for expected points across branches while amplifying inconsistencies for anomalies. An asymmetric branch design further prevents model collapse by maintaining distinct cen-

ter vectors across branches, enabling robust self-supervised learning. This framework enhances generalization to unseen anomalies by focusing on latent pattern differences rather than prior knowledge of anomaly characteristics. However, DCdetectors suffer from several problems. One is the sensitivity to contrastive sample quality, which degrades performance on imbalanced or poorly separable data. In addition to that, the high computational overhead from pairwise comparisons and dual-branch parallelism remain issues.

Building upon these foundations, we propose MAAT (Mamba Adaptive Anomaly Transformer with association discrepancy for time series) for anomaly detection in time series. Our approach introduces a novel block architecture that incorporates skip connections and gating mechanisms in association with the mamba block in the skip connection to improve the reconstruction capability of the anomaly transformer architecture. By combining these architectural enhancements with sparse attention mechanisms, Anomaly Transformer association modeling principles, MAAT achieves superior performance in detecting anomalies across diverse datasets.

The Key contributions of this work are summarized as follows:

- integrated sparse attention mechanisms to replace the standard attention mechanism in the original Anomaly Transformer, allowing scalable and efficient processing of long time series data. By enabling dynamic control over block size, MAAT achieves an optimal balance between computational efficiency and precision in anomaly detection.
- Introduced the MAMBA block to the Anomaly Transformer architecture to optimize the reconstruction of signals.
- Incorporated the MAMBA block with skip connections and gating attention to enhance the reconstruction output and reduce the loss of the Anomaly Transformer architecture.

The subsequent sections of this document are structured as follows: Section 2 presents a comprehensive overview of relevant works, including literature and methodologies, related to time series anomaly detection. Section 3 delves into our proposed MAAT architecture, detailing its unique features and potential benefits. In Section 4, we conduct Experiments, perform data analysis and provide a thorough evaluation of our model. Lastly, in Section 5, we draw insightful conclusions based on the following: In our experimentation, we compare our approach with prior methodologies and articulate

the implications of our findings. This structure ensures a coherent and comprehensive understanding of our innovative methodology for unsupervised anomaly detection in time series data.

2. Related works

Time series anomaly detection has significantly advanced over the past few decades, progressing from traditional statistical models to cutting-edge deep learning and Transformer-based architectures. This section provides a detailed review of the evolution of these methods, with a particular focus on recent developments. Early time series anomaly detection work was dominated by classical statistical models such as ARIMA and Gaussian Processes (GP). ARIMA was widely used for detecting anomalies as deviations from expected values based on assumptions of linearity and stationarity [3]. However, these models were ill-suited to handle non-linear and complex patterns in real-world data. Gaussian Processes added a probabilistic framework, allowing uncertainty quantification in predictions [?]. Despite these improvements, ARIMA and GP struggled with high-dimensional and multivariate data, limiting their effectiveness in more complex financial and industrial monitoring applications. The rise of machine learning models has introduced more flexible approaches. Support Vector Machines (SVMs), particularly the One-Class SVM (OC-SVM), became popular for novelty detection, learning a decision boundary that encloses expected data points while flagging outliers as anomalies [4]. Despite improving over traditional statistical methods, SVMs required extensive feature engineering and could not capture temporal dependencies inherent in sequential data. Random Forests and Isolation Forests introduced new paradigms by leveraging decision trees to detect anomalies. Random Forests required fewer assumptions and handled high-dimensional data better than SVMs, while Isolation Forests identified anomalies by isolating points through recursive partitioning [18]. Both methods, however, focused on pointwise anomalies and were not optimized for capturing time dependencies in sequential data. Probabilistic methods like Hidden Markov Models (HMMs) introduced temporal dynamics into anomaly detection. HMMs model a system transitioning between hidden states over time, detecting anomalies as deviations in state transitions [5]. While HMMs represented a significant step forward, they were still limited in handling non-linear patterns and required substantial computational resources for larger datasets. The emergence of deep learning marked a significant shift in time

series anomaly detection. Recurrent Neural Networks (RNNs), and more specifically, Long Short-Term Memory (LSTM) networks, became popular due to their ability to capture long-term dependencies in time series data [6]. These models excelled in detecting anomalies in healthcare (e.g., ECG data) and finance [19], where subtle deviations from standard patterns need to be identified. However, RNNs and LSTMs face limitations in scalability and can struggle with vanishing gradient problems when processing long sequences. Autoencoders (AEs), particularly Variational Autoencoders (VAEs), became central to unsupervised anomaly detection by reconstructing standard data patterns and flagging high-reconstruction errors as anomalies [11]. Adversarial Autoencoders (AAEs) and Generative Adversarial Networks (GANs) introduced adversarial training, improving the robustness of anomaly detection models. GANs, in particular, used a generator and discriminator framework to detect anomalies based on how well the model could generate realistic data samples. However, GANs and AEs both require large amounts of data for training and can suffer from instability, making them challenging to apply in certain domains [20, 21]. More recently, Transformer-based models have demonstrated significant potential in time series anomaly detection, driven by their ability to capture long-range dependencies through self-attention mechanisms. Initially developed for natural language processing tasks, transformers have been successfully applied to time series analysis without the need for recurrent structures like those in RNNs or LSTMs. The self-attention mechanism allows Transformers to capture local and global dependencies within time series data, enabling them to detect various anomaly types [13]. One prominent model is the Anomaly Transformer, which introduced the novel concept of Association Discrepancy to identify anomalies by comparing expected associations in time series data with observed ones. Using a minimax strategy, the Anomaly Transformer improves the distinguishability between normal and abnormal points, outperforming previous models across various datasets [16]. Its success highlights the growing importance of attention mechanisms in detecting complex temporal patterns, especially in high-dimensional datasets such as those found in industrial or sensor data. Several Transformer variants have emerged in recent years, each building on the strengths of the original Transformer architecture. AnomalyBERT is a model that uses self-supervised learning and a data degradation scheme to synthesize outliers and train the model to detect them. By simulating various types of anomalies, AnomalyBERT improves its ability to generalize to unseen anomalies without relying on labeled datasets [22].

Similarly, the Denoising Diffusion Mask Transformer (DDMT) combines denoising diffusion models with Transformers to enhance anomaly detection in multivariate time series, particularly in noisy environments. DDMT employs a masking mechanism to prevent information leakage, significantly improving performance in noisy industrial datasets [23]. The ongoing evolution of these models has also addressed the challenge of multivariate anomaly detection, where multiple time series are analyzed simultaneously to detect correlated anomalies. Models like Informer [24] and multi-task Transformers have been applied to multivariate settings, leveraging attention mechanisms to model dependencies between multiple variables effectively [25]. Hybrid models that combine the strengths of statistical models and deep learning are also emerging, offering improved interpretability while retaining the flexibility of neural networks. Early approaches to unsupervised time series anomaly detection primarily relied on classical statistical methods such as ARIMA models and hypothesis tests, laying the groundwork for distinguishing normal from abnormal behavior. However, these traditional methods were often limited by their inability to capture the complex interdependencies and non-stationarities inherent in high-dimensional, multivariate time series data. As the field progressed, deep learning frameworks began to emerge. In 2021, the **Anomaly Transformer** [16] introduced a novel anomaly-attention mechanism that quantifies the association discrepancy between normal and abnormal points. While this approach effectively leverages self-attention to capture both local and global temporal dependencies in an unsupervised manner, its quadratic complexity poses challenges for scalability, and its underlying assumptions may not hold across all types of anomalies. Building on these advances, the **DC Detector** [17] employs a dual attention contrastive representation learning framework. Integrating local and global attention with a contrastive loss overcomes some of the pitfalls of reconstruction-based methods. Nonetheless, the additional architectural complexity and the need for extensive hyperparameter tuning remain nontrivial hurdles. Concurrently, selective state space models have gained traction for their efficiency. Models like **MAMBA** [26] use a selective scanning mechanism to model long-range dependencies linearly, making them attractive for real-time and large-scale applications. However, the trade-off is a potential flexibility reduction when modeling highly non-linear interactions. Despite these significant advances, several challenges persist. One major issue is **concept drift**, the phenomenon where the underlying distribution of data evolves. This drift renders pre-trained models ineffective and highlights the need for adaptive

learning techniques that can update dynamically as new data becomes available. In addition, scalability remains a critical challenge, especially when dealing with high-frequency time series data or real-time anomaly detection in large-scale systems. Recent efforts in developing memory-efficient Transformers and distributed learning approaches [27, 28] have begun to address these scalability issues, marking promising steps toward more adaptive and robust anomaly detection systems. Overall, the evolution of unsupervised time series anomaly detection reflects a broader trajectory across complex domains. The field is steadily progressing toward more nuanced, robust, and adaptable solutions, from early statistical methods to modern deep learning architectures that harness attention mechanisms, contrastive learning, and efficient state space representations. These advancements enhance our ability to capture intricate temporal dependencies and subtle deviations without relying on labeled data and pave the way for deploying these models in real-world, dynamic environments.

3. Methodology

Consider a system that records a sequence of d -dimensional measurements at uniform time intervals. The time series data is represented by the set $\{x_1, x_2, \dots, x_N\}$, where each $x_t \in \mathbb{R}^d$. The goal is to determine whether an observation x_t is anomalous in an unsupervised manner. Effective unsupervised time series anomaly detection relies on learning informative representations and establishing a clear discriminative criterion. The original Anomaly Transformer framework achieved this by learning an association discrepancy that distinguishes standard patterns from anomalies through anomaly attention and a minimax optimization strategy. The Mamba Adaptive Anomaly Transformer (MAAT) builds upon the Anomaly Transformer by introducing computationally efficient Anomaly Sparse Attention, Mamba Blocks, and Gated Skip Connections. This hybrid approach enhances short-range dependency modeling and long-range temporal learning while reducing computational costs. As illustrated in Figure 1(A), Anomaly Sparse Attention replaces dense self-attention with a two-branch mechanism. The Prior-Association Branch encodes expected dependencies using a learnable Gaussian kernel, while the Series-Association Branch applies block-wise sparse attention to capture time series patterns adaptively. These associations guide discrepancy learning, enhancing anomaly detection performance. The Reconstruction Block, shown in Figure 1(B), refines extracted features by stacking

MAAT Blocks with LayerNorm and Feed-Forward Networks (FFN). This layered design supports hierarchical feature learning, making the model more robust to diverse time series behaviors. Finally, the MAAT Block, depicted in Figure 1(C), integrates Mamba Blocks within a Gated Attention mechanism, selectively amplifying meaningful signals while filtering out noise, and the skip connection preserves critical information while adapting the model focus. MAAT provides a scalable and expressive framework for detecting complex anomalies across various time series datasets by combining sparse attention, state-space modeling, and gated learning mechanisms with the association discrepancy. Algorithm 1 summarizes the overall computation flow of MAAT, detailing how Anomaly Sparse Attention, Mamba Blocks, and Gated Skip Connections interact to refine the features for anomaly detection.

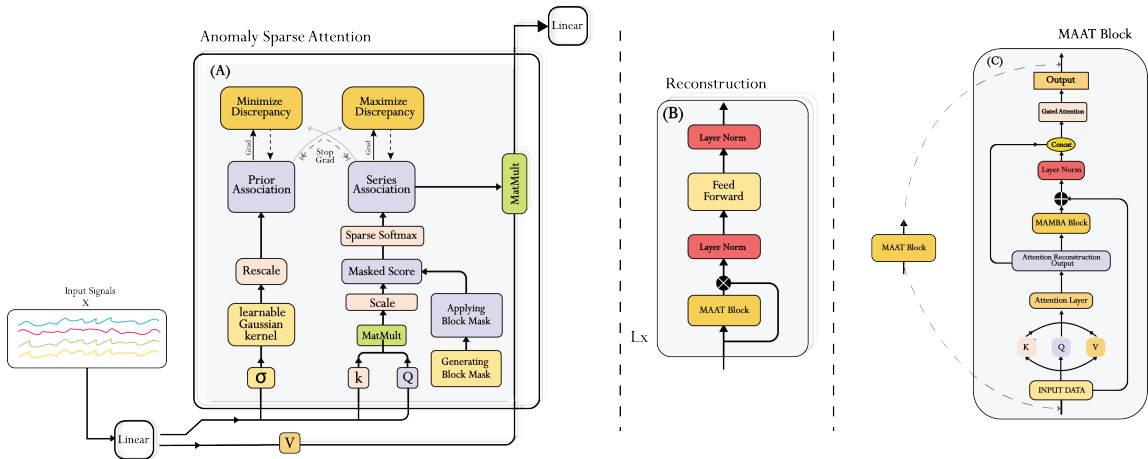


Figure 1: The figure illustrates the MAAT framework for time series anomaly detection. Block A (Anomaly Sparse Attention Module) computes prior and series associations using sparse attention and a learnable Gaussian kernel to model temporal dependencies. Block B (Reconstruction Module) refines the feature representations using layer normalization, feedforward processing, and MAAT blocks to reconstruct input signals effectively. Block C represents the MAAT Block that integrates the Mamba state-space model to capture long-range dependencies, followed by a gated attention mechanism that adaptively fuses the reconstructed output.

Algorithm 1 MAAT: Mamba Adaptive Anomaly Transformer with Sparse Attention

Require: Time series $x \in \mathbb{R}^{B \times L \times D}$
Require: Parameters: $block_size$, d_model , n_heads , e_layers , d_state , d_conv
Ensure: Reconstruction x , Anomaly scores: $series$, $prior$, σ

- 1: Initialize $series_list \leftarrow \emptyset$, $prior_list \leftarrow \emptyset$, $\sigma_list \leftarrow \emptyset$
- 2: $x_{orig} \leftarrow x$ ▷ Preserve initial input
- 3: **for** $i = 1$ to e_layers **do**
- 4: **Sparse Attention Processing:**
- 5: $x, series, prior, \sigma \leftarrow \text{sparse_attn_layer}(x, block_size, attn_mask)$ ▷ Compute sparse block-wise attention over windows of size $block_size$
- 6: **Mamba Skip Path:**
- 7: $x_{mamba} \leftarrow \text{MambaBlock}(x)$ ▷ State-space model capturing long-range dependencies
- 8: $x_{skip} \leftarrow x_{mamba} + x_{orig}$ ▷ Residual connection
- 9: $x_{skip} \leftarrow \text{LayerNorm}(x_{skip})$
- 10: **Adaptive Gating:**
- 11: $g \leftarrow \sigma(\text{Linear}([x; x_{skip}]))$ ▷ Gated feature fusion
- 12: $x \leftarrow g \odot x_{skip} + (1 - g) \odot x$ ▷ Learnable blend of skip and main path
- 13: **State Update:**
- 14: $x_{orig} \leftarrow x$ ▷ Update input for next layer
- 15: Append $series$ to $series_list$
- 16: Append $prior$ to $prior_list$
- 17: Append σ to σ_list
- 18: **end for**
- 19: **if** $\text{norm} \neq \text{None}$ **then**
- 20: $x \leftarrow \text{LayerNorm}(x)$
- 21: **end if**
- 22: **return** $x, series_list, prior_list, \sigma_list$

3.1. Background knowledge

3.1.1. Association Discrepancy

The association discrepancy (AssDis) metric quantifies the mismatch between the **prior-association** (P) and the **series-association** (S). The prior-association mechanism models temporal dependencies using a learnable Gaussian kernel, where nearby time steps receive higher weights. The association score between steps i and j in layer l is computed and normalized as:

$$P_{i,j}^l = \frac{1}{\sqrt{2\pi}\sigma_i} \exp\left(-\frac{(j-i)^2}{2\sigma_i^2}\right), \quad P_{i,:}^l = \text{Softmax}(P_{i,:}^l), \quad (1)$$

where σ_i is a learnable scale parameter controlling the temporal influence range.

The series association $S_{i,j}$ represents the observed dependencies between time points using standard self-attention, which computes global attention scores for all pairs of time points. It is defined as:

$$S_{i,j} = \frac{\exp\left(\frac{Q_i K_j^T}{\sqrt{d_{\text{model}}}}\right)}{\sum_{k=1}^T \exp\left(\frac{Q_i K_k^T}{\sqrt{d_{\text{model}}}}\right)}, \quad (2)$$

where Q_i and K_j are the query and key vectors for the i -th and j -th time points, respectively, d_{model} is the dimensionality of the model, used to scale the dot product for numerical stability, and T is the total number of time points in the sequence.

- The **prior-association** (P) captures expected temporal patterns via Gaussian kernels
- The **series-association** (S) encodes actual dependencies through localized attention
- Their discrepancy reveals alignment between expected and observed temporal relationships

The association discrepancy (AssDis) is computed as symmetric KL divergence:

$$\text{AssDis}(P, S; X) = \frac{1}{L} \sum_{l=1}^L \left[\sum_{i=1}^N \text{KL}(P_{i,:}^l \parallel S_{i,:}^l) + \text{KL}(S_{i,:}^l \parallel P_{i,:}^l) \right], \quad (3)$$

- $\text{KL}(P \parallel S)$ measures deviation of observed dependencies from expectations
- Reverse $\text{KL}(S \parallel P)$ prevents mode collapse in divergence measurement
- Symmetric formulation ensures balanced comparison of distributions

3.1.2. Minimax Optimization

The Anomaly Transformer framework employs a minimax optimization strategy that alternates between two phases to balance the learning of two complementary feature sets, P and S . This alternating approach prevents collapse in the representation of P while ensuring that S captures non-local dependencies.

Minimize Phase: In this phase, the parameters responsible for generating P are updated while S is kept fixed (detached). The loss function is defined as:

$$\mathcal{L}_{\text{Min}} = \|X - \hat{X}\|_2^2 - \lambda \cdot \text{AssDis}(P, S_{\text{detach}}; X), \quad (4)$$

Where:

- $\|X - \hat{X}\|_2^2$ is the reconstruction loss that ensures the input X is accurately reconstructed.
- $\text{AssDis}(P, S_{\text{detach}}; X)$ is the association discrepancy term, which quantifies the dissimilarity between the feature set P and a detached version of S . Detaching S prevents its gradients from being updated, providing a stable target for P .
- λ is a hyperparameter that controls the trade-off between the reconstruction loss and the association discrepancy.

This phase drives P to learn diverse, fine-grained local features while discouraging trivial or collapsed representations.

Maximize Phase: In this phase, the parameters generating S are updated while P is held fixed (detached). The corresponding loss function is given by:

$$\mathcal{L}_{\text{Max}} = \|X - \hat{X}\|_2^2 + \lambda \cdot \text{AssDis}(P_{\text{detach}}, S; X), \quad (5)$$

Where:

- The reconstruction loss $\|X - \hat{X}\|_2^2$ remains in place to ensure accurate reconstruction of the input X .
- $\text{AssDis}(P_{\text{detach}}, S; X)$ measures the association discrepancy between a detached P and S , encouraging S to capture non-local, global dependencies that complement the local features encoded in P .
- λ again regulates the relative importance of the association discrepancy term.

Adversarial Strategy: The alternating updates between the two phases create an adversarial learning mechanism:

- In the **Minimize Phase**, P is encouraged to develop informative and diverse local representations.
- In the **Maximize Phase**, S is optimized to extract non-local, contextual dependencies.

As introduced in the Anomaly Transformer framework, this minimax strategy ensures that both feature sets capture complementary aspects of the input data, enhancing the overall quality of the learned representations. The hyperparameter λ is critical in balancing the network ability to reconstruct the input with the need for diverse and informative feature learning.

3.1.3. Association-based Anomaly Criterion

The Anomaly Transformer framework integrates temporal pattern analysis with reconstruction fidelity through a dual-mechanism scoring system. The final anomaly score for an input $X \in \mathbb{R}^{N \times d}$ is computed as:

$$\text{AnomalyScore}(X) = \text{Softmax}\left(-\text{AssDis}(P, S; X)\right) \odot \|X_{i,:} - \hat{X}_{i,:}\|_2^2, \quad i = 1, \dots, N, \quad (6)$$

Where:

- $\text{AssDis}(P, S; X)$ measures the association discrepancy between prior-association (P) and series-association (S),
- $\text{Softmax}(\cdot)$ normalizes the negative association discrepancy across time steps,
- \odot represents element-wise multiplication,

- $\|X_{i,:} - \hat{X}_{i,:}\|_2^2$ quantifies the reconstruction error at each time step i .

This formulation leverages both temporal dependency patterns and reconstruction accuracy for anomaly detection. While improved reconstructions generally reduce the association discrepancy, anomalies may still yield high scores due to significant deviations in either reconstruction error or temporal patterns. The probabilistic weighting ensures that time steps exhibiting both poor reconstruction and abnormal dependencies are emphasized, enhancing detection robustness.

3.2. Sparse Attention for Efficient Sequence Processing

Standard self-attention in Transformer architectures computes interactions between every pair of tokens, resulting in a quadratic computational complexity of $O(N^2)$. To mitigate this, sparse attention restricts token interactions by applying a sparsity pattern S that selects only a subset of pairs for attention computation [29, 30, 31].

In conventional self-attention, the operation is defined as:

$$\text{Attention}(Q, K, V) = \text{softmax} \left(\frac{QK^T}{\sqrt{d_k}} \right) V, \quad (7)$$

Where:

- $Q, K, V \in \mathbb{R}^{N \times d}$ are the query, key, and value matrices,
- d_k denotes the dimensionality of the key vectors,
- The softmax function normalizes the attention scores.

Sparse attention introduces a sparsity mask S to limit interactions:

$$\text{SparseAttention}(Q, K, V) = \text{softmax} \left(\frac{(QK^T) \odot S}{\sqrt{d_k}} \right) V, \quad (8)$$

where \odot represents element-wise multiplication. This ensures that only selected token pairs contribute to the attention mechanism.

Approaches for defining the sparsity pattern S include:

- **Fixed Patterns:** Predefined structures, such as strided or block-wise masks [29].

- **Learned Masks:** Patterns that are dynamically optimized during training [30].
- **Memory-Efficient Methods:** Techniques like locality-sensitive hashing (LSH) that enable content-based token selection [31].

3.3. Gated Attention Mechanism

The gated attention mechanism enhances standard attention by dynamically adjusting the importance of features through learnable gating. Rather than treating all input features equally, it evaluates their relevance to suppress or amplify contributions, optimizing attention weight distribution. Mathematically, this is expressed as:

$$\text{GatedAttention}(x) = \sigma(G(x)) \odot A(x), \quad (9)$$

Where:

- x is the input data,
- $G(x)$ is a neural network-generated gating vector,
- σ (sigmoid) maps gating values to $[0, 1]$,
- $A(x)$ denotes standard attention weights,
- \odot signifies element-wise multiplication.

The model selectively prioritizes task-critical features while suppressing noise by modulating the attention mechanism with context-sensitive gates. This adaptability improves robustness in scenarios such as anomaly detection, where distinguishing relevant signals from irrelevant background patterns is essential.

3.4. Mamba State Space Model

State Space Models (SSMs) are widely used in time series modeling because they capture latent dynamics efficiently. The **Mamba State Space Model (Mamba SSM)** is a recent advancement in structured state-space models (S4) designed for long-range sequence modeling while maintaining computational efficiency [32, 33]. The following equations define Mamba SSM:

3.4.1. State Update Equation

$$x_{t+1} = Ax_t + Bu_t \quad (10)$$

Where:

- x_t represents the hidden state at time t ,
- A is the state transition matrix,
- B is the input matrix,
- u_t represents the external input.

The observation equation connects the underlying system dynamics to the measurable signal. It ensures that latent states, which capture long-range dependencies, are projected onto the observed space.

3.5. Mamba Adaptive Anomaly Transformer Architecture

Figure 1 illustrates the overall structure of the Mamba Adaptive Anomaly Transformer (MAAT), an architecture inspired by the Anomaly Transformer. MAAT integrates a sparse attention mechanism, a selective state-space model known as the Mamba block, and an adaptive reconstruction framework. The sparse attention mechanism processes the input time series data, capturing local dependencies efficiently. The Mamba block is designed to capture long-range dependencies, enhancing the model ability to understand complex temporal patterns. An adaptive gating mechanism then fuses the outputs from the sparse attention and Mamba block, enabling the model to reconstruct the input signal effectively. This combination allows MAAT to detect anomalies by comparing the reconstructed signal with the original input, identifying deviations that may indicate anomalous behavior.

3.5.1. Anomaly sparse attention

Our anomaly sparse attention module, shown in Figure 1(A), refines the conventional anomaly attention used in the Anomaly Transformer, which relies on selfattention, by incorporating sparse attention. While the prior-association remains unchanged, modeled using a learnable Gaussian kernel Eq. (1), the series-association is now computed through sparse self-attention Eq. (2), capturing observed dependencies more efficiently.

In this module, the prior association continues to be represented by a learnable Gaussian kernel, while the series association is computed using a sparse softmax operation over local attention windows.

For each query vector Q_i , normalization is performed only over keys in the local window defined by

$$\Omega_i = \{j \mid |j - i| \leq \text{block_size}/2\}, \quad (11)$$

so that the series association is computed as

$$S_{i,j}^l = \frac{\exp\left(\frac{Q_i K_j^T}{\sqrt{d_{\text{model}}}}\right)}{\sum_{k \in \Omega_i} \exp\left(\frac{Q_i K_k^T}{\sqrt{d_{\text{model}}}}\right)}, \quad \forall j \in \Omega_i, \quad (12)$$

with

$$S_{i,j}^l = 0 \quad \text{for } j \notin \Omega_i. \quad (13)$$

This sparse softmax formulation ensures that only locally relevant keys are considered during normalization, reducing computational redundancy while preserving essential dependencies.

3.5.2. MAAT Adaptive Block

The adaptive block shown in Figure 1(C) integrates a state-space model (Mamba block) with a skip connection that retains the original input. The Mamba block is specifically designed to capture long-range dependencies, while the skip connection ensures the preservation of fine details. We achieve a robust intermediate representation by combining these elements and applying layer normalization. This Adaptive Block merges long-range dependencies and local features through a state-space (Mamba) skip path and an adaptive gating mechanism. After performing sparse attention processing, we proceed with the following steps: The Mamba block generates a transformed representation x_{mamba} , which is then combined with the reconstructed input from sparse attention x_{orig} via a residual connection. This output is normalized as follows:

$$x_{\text{skip}} = \text{LayerNorm}(x_{\text{mamba}} + x_{\text{orig}}), \quad (14)$$

Adaptive Gating and Reconstruction: In the context of adaptive gating and reconstruction, a gating factor g is computed from the concatenation of the

output from the central processing path x and the corresponding skip connection x_{skip} . Formally, the gating factor can be expressed as follows:

$$g = \sigma(\text{Linear}([x; x_{\text{skip}}])) = \sigma(W[x; x_{\text{skip}}] + b), \quad (15)$$

Where $[x; x_{\text{skip}}]$ denotes the concatenation of the feature maps along the channel dimension, W and b represent the learnable parameters of the linear transformation (precisely, the weight matrix and bias term), and $\sigma(\cdot)$ is the sigmoid activation function that maps the output to the range $(0, 1)$.

The gating factor g is critical in modulating the relative importance of the skip and main paths. Specifically, for each element:

- When g approaches 1, the output is predominantly influenced by the skip connection x_{skip} , which encapsulates long-range contextual information along with a residual signal from the original input.
- Conversely, when g approaches 0, the reconstruction is primarily derived from the main path output x , which reflects the locally processed features.

The final output, denoted as X^{adapt} , is computed as an element-wise weighted combination of these two representations:

$$X^{\text{adapt}} = g \odot x_{\text{skip}} + (1 - g) \odot x, \quad (16)$$

where \odot signifies element-wise multiplication. This formulation enables the network to dynamically calibrate the contributions from the skip connection and the main processing branch, thereby facilitating a harmonious integration of local details and global context. The process of adaptive fusion is paramount in ensuring that the reconstructed output X^{adapt} accurately embodies normal patterns. In contrast, anomalies disrupt local consistency and global structure, increasing reconstruction errors. This enhanced reconstruction capability, in turn, fosters improved performance in anomaly detection.

Consequently, X^{adapt} represents a sophisticated integrated reconstruction, merging information from both the skip path and the central processing branch, ultimately enhancing the overall representational capacity of the model.

The anomaly score now leverages the adaptively fused reconstruction X^{adapt} by balancing the association discrepancy from Eq. (17) and the reconstruction error. Specifically, the anomaly score for each time step i is defined

as

$$\text{AnomalyScore}(X) = \text{Softmax}\left(-\text{AssDis}(P, S; X)\right) \odot \left\|X_{i,:} - X_{i,:}^{\text{adapt}}\right\|_2^2, \quad i = 1, \dots, N. \quad (17)$$

Here, \odot represents element-wise multiplication, and:

- $\text{AnomalyScore}(X) \in \mathbb{R}^{N \times 1}$ provides the point-wise anomaly criterion.
- $\text{AssDis}(P, S; X)$ is the association discrepancy, as defined in Eq. (17).
- $\|X_{i,:} - X_{i,:}^{\text{adapt}}\|_2^2$ is the reconstruction error between the input X and its adaptively reconstructed counterpart X^{adapt} .

This updated formulation clearly distinguishes the adaptively reconstructed output X^{adapt} , which utilizes the gating for reconstruction from the input X , emphasizing the role of adaptive fusion in our anomaly detection criterion.

4. Experiments

4.1. Benchmark Datasets

In this study, we evaluate the performance of our model using eight representative benchmarks derived from five real-world applications. The first dataset, MSL, is the Mars Science Laboratory dataset collected by NASA, which reflects the condition of sensors and actuator data from the Mars rover [34]. Similarly, the SMAP dataset, provided by NASA, presents soil samples and telemetry information from the Mars rover; notably, SMAP contains more point anomalies than MSL [35]. The PSM dataset, a public resource from eBay Server Machines, includes 25 dimensions and is widely used for research in anomaly detection [36]. Additionally, the SMD dataset consists of a five-week-long record of resource utilization traces collected from an internet company compute cluster, monitoring 28 machines [37]. Another critical benchmark is the SWaT dataset, which comprises 51-dimensional sensor data from a secure water treatment system that operates continuously [38]. Furthermore, the NIPS-TS-SWAN dataset provides a comprehensive multivariate time series benchmark extracted from solar photospheric vector magnetograms in the Spaceweather HMI Active Region Patch series [39]. Lastly, the NIPS-TS-GECCO dataset is a drinking water quality dataset for the Internet of Things, published in the 2018 Genetic and Evolutionary Computation Conference [40].

4.2. Implementation

Our study uses the same protocol as the Anomaly Transformer model to assess our approach efficacy. We generate sub-series using a non-overlapping sliding window technique, with most datasets using a fixed window size of 100, while the SMAP dataset uses a size of 105. Anomaly detection involves assigning scores to time points and setting a threshold based on the "Anomaly Ratio" in Table 1. The batch size varies from 32 to 256 for optimization. We maintain a model dimensionality of 512 for balance and use the ADAM optimizer with early stopping during training. This methodology provides a robust framework for evaluating our approach against existing techniques while ensuring reproducibility and highlighting our improvements.

Table 1: Hyperparameters for MAAT model across Datasets

Dataset	Window Size	Batch Size	d_{model}	Anomaly Ratio (%)
SMD	100	128	512	0.5
MSL	100	256	512	0.85
SMAP	105	128	512	0.5
PSM	100	128	512	1
SWaT	100	256	512	0.5
NIPS-TS-GECCO	100	32	512	0.5
NIPS-TS-SWAN	100	128	512	0.9

4.3. Evaluation Metrics

Evaluating anomaly detection in time series data requires metrics assessing point-wise performance and capturing anomalies' temporal continuity. This work uses traditional and specialized point-based metrics to evaluate contiguous anomaly segments.

4.3.1. Point-Based Metrics

The standard metrics include Precision, Recall, and F1 Score, calculated using the counts of true positives (TP), false positives (FP), and false negatives (FN). The F1 Score is the harmonic mean of Precision and Recall [41].

4.3.2. Affiliation Metrics: $\text{Aff-}P$ and $\text{Aff-}R$

These metrics evaluate partial detection within multi-step anomaly segments.

Affiliation Precision (Aff-P): Measures the fraction of predicted anomalies within true anomaly ranges:

$$\text{Aff-P} = \frac{\sum_{t \in \mathcal{P}} \mathbf{1}\{t \in \mathcal{T}\}}{|\mathcal{P}|}, \quad (18)$$

where \mathcal{P} is the predicted anomalies, \mathcal{T} is the true anomalies, and $\mathbf{1}\{\cdot\}$ is the indicator function.

Affiliation Recall (Aff-R): Measures the fraction of true anomalies detected:

$$\text{Aff-R} = \frac{\sum_{t \in \mathcal{T}} \mathbf{1}\{t \in \mathcal{P}\}}{|\mathcal{T}|}. \quad (19)$$

4.3.3. Range-Based Metrics

These assess detection over entire anomaly segments.

Range-based Anomaly Recall (R_A_R): A true anomaly range R_i^{true} is detected if overlap with any predicted range exceeds threshold τ :

$$\text{R_A_R} = \frac{\sum_{i=1}^{N_{\text{true}}} \mathbf{1}\left\{ \max_j \text{Overlap}(R_i^{\text{true}}, R_j^{\text{pred}}) \geq \tau \right\}}{N_{\text{true}}}. \quad (20)$$

Range-based Anomaly Precision (R_A_P):

$$\text{R_A_P} = \frac{\sum_{j=1}^{N_{\text{pred}}} \mathbf{1}\left\{ \max_i \text{Overlap}(R_j^{\text{pred}}, R_i^{\text{true}}) \geq \tau \right\}}{N_{\text{pred}}}. \quad (21)$$

4.3.4. Volume-Based Metrics: V_ROC and V_PR

These incorporate anomaly duration into evaluation.

Volume-based ROC (V_ROC): Adjusts TPR and FPR by anomaly volume:

$$\text{TPR}_{\text{vol}} = \frac{\text{Volume of Correct Detections}}{\text{Total Volume of True Anomalies}}, \quad \text{FPR}_{\text{vol}} = \frac{\text{Volume of False Detections}}{\text{Total Volume of Normal Data}}.$$

The V_ROC curve plots TPR_{vol} vs. FPR_{vol} .

Volume-based Precision-Recall (V_PR): Defines volume-weighted precision and recall:

$$\text{Precision}_{\text{vol}} = \frac{\text{Volume of Correct Detections}}{\text{Volume of All Detections}}, \quad \text{Recall}_{\text{vol}} = \frac{\text{Volume of Correct Detections}}{\text{Total Volume of True Anomalies}}.$$

The V_PR curve plots $\text{Precision}_{\text{vol}}$ vs. $\text{Recall}_{\text{vol}}$.

In summary, while point-based metrics offer a basic assessment, affiliation, range-based, and volume-based metrics (18, 19, 20, 21) provide a comprehensive evaluation by accounting for temporal structure and anomaly duration [42, 43].

5. Results

5.1. Baseline Results

After conducting various experiments, we present our results evaluated on precision Recall and F1 score metrics in Table 2: Our model Achieves remarkable improvements over existing methods, particularly when compared to the DCdetector and Anomaly Transformer, two leading approaches in the field. For instance,

On the **SMD** dataset, which consists of highly non-stationary multivariate time series with intricate temporal dependencies, our proposed model achieves an F1-score of **92.30%**. This performance surpasses the Anomaly Transformer by an absolute margin of **+2.18%** and outperforms DCdetector by **+8.64%**. Furthermore, our model demonstrates a notable improvement in Recall, achieving **+3.84%** higher than the Anomaly Transformer and **+13.93%** higher than DCdetector, while also exhibiting enhancements in Precision by **+0.63%** and **+3.74%**, respectively.

On the **MSL** dataset, our model attains an F1-score of **95.05%**, yielding an absolute improvement of **+1.19%** over the Anomaly Transformer and **+0.32%** over DCdetector. In addition, our approach achieves a **+2.40%** increase in Recall compared to the Anomaly Transformer and **+0.95%** compared to DCdetector, while demonstrating a **+1.14%** enhancement in Precision relative to the Anomaly Transformer, with a minor decrease of **0.21%** when compared to DCdetector. Similarly, on the **SMAP** dataset, our method achieves an F1-score of **96.99%**, demonstrating an absolute gain of **+0.60%** over the Anomaly Transformer and **+0.93%** over DCdetector. Our model also attains a **+1.24%** improvement in Precision over the Anomaly Transformer and **+0.49%** over DCdetector. Meanwhile, Recall exhibits a marginal

decrease of **0.08%** compared to the Anomaly Transformer, but an increase of **+1.39%** relative to DCdetector. On the **SWaT** dataset, our model achieves an F1-score of **96.50%**, outperforming the Anomaly Transformer by **+0.09%** and DCdetector by **+0.08%**. While our model exhibits a **0.28%** reduction in Precision compared to the Anomaly Transformer, it surpasses DCdetector by **+0.23%**. Additionally, our method improves Recall by **+0.59%** relative to the Anomaly Transformer and by **+0.04%** compared to DCdetector. Finally, on the **PSM** dataset, our model achieves an F1-score of **98.32%**, demonstrating an improvement of **+0.87%** over the Anomaly Transformer and **+0.50%** over DCdetector. Precision is enhanced by **+0.35%** and **+0.27%** relative to the Anomaly Transformer and DCdetector, respectively, while Recall is increased by **+1.39%** and **+0.73%**, respectively.

Despite these successes, there are instances where MAAT exhibits slightly lower performance compared to specific methods. For example, on the **MSL** dataset, while MAAT outperforms Anomaly Transformer and closely matches DCdetector, its precision (**92.06%**) is marginally lower than DCdetector (**92.25%**), representing a decrease of **0.19%**. This minor discrepancy may stem from DCdetector dual-attention contrastive learning approach, which appears to excel in precision for datasets with high variability. Additionally, on the **SWaT** dataset, MAAT achieves a recall of **100.00%**, matching DCdetector, but its precision is slightly lower than DCdetector, representing a decrease of **0.26%**. These small trade-offs highlight areas where further optimization could enhance MAAT performance, particularly when precision is prioritized over recall.

In Table 3 ,Our model establishes a new benchmark for anomaly detection on the NIPS-TS-GECCO and NIPS-TS-SWAN datasets, surpassing the best-performing methods in most metrics while demonstrating exceptional robustness across diverse challenges.

On the **NIPS-TS-GECCO** dataset, our model achieves an F1-score of **52.8%**, significantly outperforming the Anomaly Transformer (27.0% F1) by an absolute margin of **+25.8%**. When compared to DCdetector, our model attains an improvement of **+6.2%** in F1, and further surpasses IForest and OCSVM by **+13.7%** (52.8% vs. 39.1%) and **+23.2%**, respectively. In terms of precision, our approach records **42.4%**, yielding a **+16.7%** gain over the Anomaly Transformer (25.7%) and a **+4.1%** improvement over DCdetector (38.3%). Although IForest exhibits a marginally higher precision of **43.9%** (a **-1.5%** difference relative to our model), this slight trade-off is offset by

Dataset	SMD			MSL			SMAP			SWaT			PSM		
	Metric	P	R	F1	P	R	F1	P	R	F1	P	R	F1	P	R
LOF	56.34	39.86	46.68	47.72	85.25	61.18	58.93	56.33	57.60	72.15	65.43	68.62	57.89	90.49	70.61
OCSVM	44.34	76.72	56.19	59.78	86.87	70.82	53.85	59.07	56.34	45.39	49.22	47.23	62.75	80.89	70.67
U-Time	65.95	74.75	70.07	57.20	71.66	63.62	49.71	56.18	52.75	46.20	87.94	60.58	82.85	79.34	81.06
Forrest	42.31	73.29	53.75	53.94	82.98	65.42	52.39	55.53	53.89	49.22	44.95	47.02	76.09	92.45	83.46
DAGMM	67.30	49.89	57.30	89.60	63.93	74.62	86.45	56.73	68.51	89.92	57.84	70.40	93.49	70.03	80.08
ITAD	86.22	73.71	79.48	69.44	84.09	76.07	82.42	66.89	73.85	63.13	52.08	57.08	72.80	64.02	68.13
VAR	78.35	70.26	74.08	71.68	81.42	77.90	81.38	53.88	64.83	81.59	60.29	69.34	90.71	83.82	87.13
MMPCACD	71.20	79.28	75.02	81.42	61.31	69.95	83.22	68.23	74.73	82.52	68.23	74.73	76.26	78.35	77.29
CL-MPPCA	82.36	76.07	79.09	73.71	88.54	80.44	63.16	72.88	67.72	76.78	81.50	79.07	56.02	99.93	71.80
TS-CP2	87.42	66.25	75.38	68.45	68.48	68.42	86.75	83.18	84.95	81.23	74.10	77.50	82.67	78.16	80.35
Deep-SVDD	78.54	79.67	79.10	91.92	76.63	83.26	56.02	69.04	62.40	80.42	84.45	82.39	95.41	86.79	90.73
BOCPD	70.90	82.04	76.07	80.32	87.60	83.62	86.45	85.85	86.14	84.96	70.75	79.01	82.72	75.33	77.70
LSTM-VAE	75.76	90.08	82.30	85.49	79.94	82.62	92.20	67.75	78.10	76.00	89.50	82.20	73.62	89.92	80.94
BeatGAN	78.55	88.92	83.42	85.42	87.88	86.64	92.38	55.85	69.61	76.04	87.46	81.32	90.30	93.84	92.04
LSTM	78.55	88.25	83.08	85.98	85.42	85.70	91.00	81.89	86.21	78.13	83.39	80.69	76.93	89.64	82.64
OmniAnomaly	83.68	88.52	85.22	90.14	89.50	89.82	81.42	84.30	82.83	81.42	84.30	82.83	83.38	74.46	78.64
THOC	79.65	91.10	85.02	88.45	90.97	89.69	92.06	89.34	90.68	92.48	98.32	95.33	97.14	98.74	97.94
AnomalyTrans	88.47	92.28	90.33	91.02	96.03	93.93	93.59	99.41	96.41	93.59	99.41	96.41	97.14	97.81	97.47
DCdetector	85.82	84.10	84.95	92.25	97.40	94.75	94.29	97.97	96.10	93.12	99.96	96.42	97.22	98.45	97.83
Ours	89.03	95.82	92.30	92.06	98.33	95.05	94.75	99.33	96.99	93.33	100.00	96.50	97.48	99.17	98.32

Table 2: Comparison of various anomaly detection metrics across different datasets

substantial gains in recall. Specifically, our model achieves a recall of **70.0%** compared to **28.5%** for the Anomaly Transformer (**+41.5%**), **59.7%** for DCdetector (**+10.3%**), and **35.3%** for IForest (**+34.7%**), while OCSVM attains a recall of **74.3%** (a **-4.3%** difference relative to our model).

On the **NIPS-TS-SWAN** dataset, our model exhibits superior performance with the highest precision (**95.9%**), recall (**59.9%**), and F1-score (**73.8%**). In particular, our model outperforms the Anomaly Transformer by **+5.2%** in precision, **+12.5%** in the recall, and **+11.5%** in F1-score. Comparisons with DCdetector reveal more modest gains of **+0.4%** in precision, **+0.3%** in recall, and **+0.4%** in F1-score. In contrast, the improvements over IForest are particularly pronounced, with an absolute increase of **+39.0%** in precision (95.9% vs. 56.9%) and **+15.5%** in F1-score. Furthermore, in comparison to OCSVM, our model demonstrates an enhancement of **+48.5%** in precision and **+25.3%** in F1-score, along with a **+10.1%** improvement in recall.

These results highlight the architectural strengths of our approach, especially the Sparse Attention mechanism and Mamba-SSM, which effectively identify subtle anomalies while reducing noise interference. Although minor trade-offs are observed specifically, a slight reduction in precision on the **NIPS-TS-GECCO** dataset and a marginal decrease in recall on the **NIPS-TS-SWAN** dataset our model consistently balances precision and recall to deliver

Table 3: Comparison of Different Methods on NIPS-TS-GECCO and NIPS-TS-SWAN Datasets

Dataset	NIPS-TS-GECCO			NIPS-TS-SWAN		
	P	R	F1	P	R	F1
MatrixProfile	4.6	18.5	7.4	17.1	17.1	17.1
GBRT	17.5	14.0	15.6	44.7	37.5	40.8
LSTM-RNN	17.0	22.6	19.3	45.2	35.8	40.0
Autoregression	39.2	31.4	34.9	42.1	35.4	38.5
OCSVM	18.5	74.3	29.6	47.4	49.8	48.5
IForest	43.9	35.3	39.1	56.9	<u>59.8</u>	58.3
AutoEncoder	42.4	34.0	37.7	47.0	52.2	50.9
AnomalyTrans	25.7	28.5	27.0	90.7	47.4	62.3
DCdetector	38.3	59.7	<u>46.6</u>	<u>95.5</u>	59.6	<u>73.4</u>
Ours	<u>42.4</u>	<u>70.0</u>	52.8	95.9	59.9	73.8

optimal overall performance.

5.2. In-Depth Performance Analysis of MAAT vs. State-of-the-Art Models

Analysis of Performance Across Datasets Refer to Table 4 The performance of our model is comprehensively evaluated against AnomalyTrans and DCdetector, two state-of-the-art methods, across five benchmark datasets: MSL, SMAP, SWaT, PSM, and SMD. The results in Table 4 demonstrate that our model consistently outperforms or closely matches the best-performing methods across most metrics, establishing its superiority in anomaly detection tasks. On the MSL dataset, our model achieves competitive results, with an F1-score of 95.05%, slightly lower than DCdetector 96.60%, representing a 1.6% decrease. However, our model surpasses AnomalyTrans in several metrics, including Accuracy Acc, where it achieves 98.92%, compared to AnomalyTrans 98.69%. While DCdetector excels in precision-related metrics such as Aff-P 51.84% and R_A_P 91.64%, our model demonstrates robust recall metrics, achieving Aff-R 96.49% and R_A_R 90.97%, which are critical for detecting subtle anomalies in noisy environments. On the SMAP dataset, our model shows slightly lower performance compared to AnomalyTrans and DCdetector. For instance, our F1-score 96.29% is marginally lower than DCdetector 97.02%, representing a 0.74% decrease. Similarly, our V ROC 92.06% and V PR 90.70% lag behind AnomalyTrans 95.52% and 93.77%, respectively. These minor trade-offs highlight areas for improvement,

particularly in precision-related metrics. Nevertheless, our model maintains strong recall metrics, such as Aff-R 94.27%, underscoring its ability to detect anomalies effectively. On the SWaT dataset, our model achieves the highest Aff-P 56.26%, surpassing both AnomalyTrans 53.03% and DCdetector 52.40%. Additionally, our model demonstrates superior recall metrics, achieving Aff-R 97.79% and R_A_R 98.14%, which are marginally higher than DCdetector 97.67% and 98.43%, respectively. Our V_ROC 98.17% and V_PR 95.02% also outperform both competitors, highlighting its robustness in handling multivariate interactions and complex temporal patterns. Our model achieves the best performance across nearly all metrics on the PSM dataset. It surpasses DCdetector in F1-score 98.32% vs. 97.94%, a 0.39% increase and Aff-P 55.53% in respect to 54.71% in Dcdetector, a 1.5% increase. Our model excels in recall-related metrics, achieving Aff-R 85.06%, R_A_R 94.15%, and R_A_P 95.09%, significantly outperforming both AnomalyTrans and DCdetector. These results underscore our model ability to handle high-dimensional sensor data with significant noise. On the SMD dataset, our model achieves the highest scores across all metrics, setting a new benchmark for performance. It surpasses AnomalyTrans in F1-score 92.30% vs. 87.18%, a 5.8% increase and Aff-P 59.19% vs. 54.36%, a 8.9% increase. Additionally, our model demonstrates superior recall metrics, achieving Aff-R 93.51%, R_A_R 79.11%, and R_A_P 75.41%, significantly outperforming both competitors. These gains highlight our model effectiveness in capturing intricate temporal patterns in highly non-stationary multivariate time series.

In this section, we will analyze its performance specifically on the **NIPS-TS-SWAN** and **NIPS-TS-GECCO** datasets, as detailed in Table 5. Our method demonstrates consistent superiority across both NIPS-TS-SWAN and NIPS-TS-GECCO benchmarks. On NIPS-TS-SWAN, our model achieves **86.10%** accuracy, outperforming AnomalyTrans by **1.53%** and DCdetector by **0.16%**. For precision, we attain **95.93%**, surpassing AnomalyTrans by **5.22%** and DCdetector by **0.45%**. The most notable gains emerge in recall, where our method improves by **12.48%** over AnomalyTrans and **0.36%** over DCdetector. These improvements translate to a **73.76% F1-score**, exceeding AnomalyTrans and DCdetector by **11.47%** and **0.41%**, respectively. On NIPS-TS-GECCO, our model achieves **98.68%** accuracy, exceeding AnomalyTrans by **0.65%** and DCdetector by **0.12%**. Precision improves dramatically by **16.76%** over AnomalyTrans and **4.16%** over DCdetector, while recall rises by **41.52%** and **10.27%**, respectively. The F1-score reflects these gains, improving by **23.73%** over AnomalyTrans and **6.19%** over DCdetec-

Table 4: Performance comparison of AnomalyTrans, DCdetector, and our method across different datasets. Best results in **bold**, second-best underlined.

Dataset	Method	Acc	F1	Aff-P	Aff-R	R_A_R	R_A_P	V_ROC	V_PR
MSL	AnomalyTrans	98.69	<u>93.93</u>	<u>51.76</u>	<u>95.98</u>	<u>90.04</u>	<u>87.87</u>	<u>88.20</u>	<u>86.26</u>
	DCdetector	99.06	96.60	51.84	97.39	93.17	91.64	95.15	91.66
	Ours	<u>98.92</u>	95.05	51.58	96.49	90.97	88.72	90.66	88.49
SMAP	AnomalyTrans	<u>99.05</u>	<u>96.41</u>	<u>51.39</u>	98.68	96.32	<u>94.07</u>	95.52	93.77
	DCdetector	99.21	97.02	51.46	<u>98.64</u>	<u>96.03</u>	94.18	<u>95.13</u>	<u>93.46</u>
	Ours	99.03	96.29	49.34	94.27	93.59	92.02	92.06	90.70
SWaT	AnomalyTrans	98.51	94.22	<u>53.03</u>	90.88	<u>97.73</u>	<u>96.32</u>	<u>97.99</u>	<u>94.39</u>
	DCdetector	99.09	96.33	52.40	<u>97.67</u>	98.43	96.96	96.95	94.34
	Ours	<u>98.97</u>	<u>95.93</u>	56.26	97.79	98.14	95.00	98.17	95.02
PSM	AnomalyTrans	98.68	97.37	<u>55.35</u>	80.85	<u>91.68</u>	<u>93.00</u>	<u>88.71</u>	<u>90.71</u>
	DCdetector	<u>98.95</u>	<u>97.94</u>	54.71	<u>82.93</u>	91.55	92.93	88.41	90.58
	Ours	99.06	98.32	55.53	85.06	94.15	95.09	90.77	92.67
SMD	AnomalyTrans	<u>98.75</u>	<u>87.18</u>	<u>54.36</u>	<u>90.12</u>	<u>74.95</u>	<u>73.00</u>	<u>78.71</u>	<u>70.71</u>
	DCdetector	98.75	84.95	51.36	88.92	70.19	65.49	68.19	63.57
	Ours	99.34	92.30	59.19	93.51	79.11	75.41	79.09	75.41

tor.

Affinity metrics further highlight our method robustness: on NIPS-TS-GECCO, **Aff-P** improves by **7.88%** over AnomalyTrans, while **Aff-R** increases by **11.89%**. Validation ROC underscores this trend, with gains of **1.55%** and **11.42%** on SWAN and GECCO, respectively, over AnomalyTrans. Collectively, these results validate our method ability to balance precision, recall, and affinity-aware performance, establishing it as a state-of-the-art solution for time-series anomaly detection.

Table 5: Multi-metric results on NIPS-TS datasets. All results in %. Best results in **bold**, second-best underlined.

Dataset	Method	Acc	P	R	F1	Aff-P	Aff-R	R_A_R	R_A_P	V_ROC
NIPS-TS-SWAN	AnomalyTrans	84.57	90.71	47.43	62.29	58.45	9.49	86.42	93.26	84.81
	DCdetector	<u>85.94</u>	<u>95.48</u>	<u>59.55</u>	<u>73.35</u>	50.48	5.63	<u>88.06</u>	<u>94.71</u>	<u>86.25</u>
	Ours	86.10	95.93	59.91	73.76	<u>58.22</u>	<u>6.72</u>	88.15	94.85	86.36
NIPS-TS-GECCO	AnomalyTrans	98.03	25.65	28.48	29.09	49.23	81.20	56.35	22.53	55.45
	DCdetector	<u>98.56</u>	<u>38.25</u>	<u>59.73</u>	<u>46.63</u>	<u>50.05</u>	<u>88.55</u>	<u>62.95</u>	<u>34.17</u>	<u>62.41</u>
	Ours	98.68	42.41	70.00	52.82	57.11	93.09	64.96	38.01	66.87

6. Discussion

6.1. Ablation Study Analysis

In this section, we introduce the ablation study of our model to highlight the importance of each block in MAAT and its impact on the baseline Anomaly Transformer model. The results of the ablation study are shown in Table 6 and Table 7. Across five datasets SMD, MSL, SMAP, SWaT, and PSM, the integration of Sparse Attention (SA), Mamba-SSM, and Gated Attention demonstrates consistent improvements over the baseline. These components work synergistically to address the challenges posed by noise, non-stationarity, and complex temporal dependencies inherent in multivariate time series data.

On the **SMD** dataset, characterized by highly non-stationary multivariate time series with intricate patterns and significant noise, the baseline Anomaly Transformer achieves a robust recall and moderate precision, yielding an F1-score in the low 90% range. However, its dense self-attention mechanism renders it susceptible to noise-induced false positives. When Sparse Attention is introduced, the model preserves its baseline precision but suffers a recall drop of approximately 2.4%, resulting in an F1 decrease of about 1.15% indicating that the block-wise formulation may oversimplify inter-variable dependencies and miss subtle anomalies. In contrast, integrating the Mamba-SSM component enhances long-range dependency capture, yet it incurs a reduction in precision by roughly 1% and a recall drop of about 2.2%, leading to an overall F1 decline of approximately 1.57%. Notably, the full MAAT model, which fuses both Sparse Attention and Mamba-SSM through a dynamic Gated Attention mechanism (Eqs. 15–16), achieves a net F1 improvement of nearly 2% over the baseline driven by a modest precision gain of around 0.6% and a substantial recall boost of roughly 3.5%. This adaptive gating effectively balances the contributions of local feature emphasis and long-term pattern refinement, robustly suppressing noise while preserving critical anomaly signals in the complex SMD environment.

For the **MSL** dataset, which consists of sensor and actuator data with high variability and transient noise, the baseline Anomaly Transformer achieves a strong recall but moderate precision, resulting in an F1-score of approximately 93.93%. However, it struggles with noise-induced false positives. The introduction of Sparse Attention mitigates this issue, leading to a precision improvement of around 0.7%, but at the cost of a 2% recall reduction, ultimately lowering the F1-score by about 1.1%. This trade-off arises as SA

effectively filters noise but inadvertently excludes short-term critical patterns. Conversely, integrating Mamba-SSM enhances precision further by approximately 1.15% over the baseline while maintaining recall stability, yielding a slight F1 improvement of 0.12%. This enhancement is attributed to Mambas ability to stabilize reconstructions via linear long-range dependency modeling. The full MAAT model synthesizes these improvements through Gated Attention, achieving an F1-score gain of 1.12% over the baselinedriven by a recall increase of 2.3% while maintaining competitive precision. During periods of transient noise, the adaptive gating mechanism (Eqs. 15) prioritizes the denoised outputs from Mamba while preserving Sparse Attentions localized anomaly signals. This balanced integration reinforces MAATs robustness to short-lived disturbances, effectively enhancing anomaly detection in highly dynamic environments.

The **SMAP** dataset, which consists of satellite telemetry data with long-range dependencies and subtle anomalies, highlights MAATs capability to balance global context with localized precision. The baseline Anomaly Transformer achieves a near-perfect recall but exhibits overfitting, limiting precision to 93.59% and resulting in an F1-score of 96.41%. To address this, Sparse Attention reduces overfitting by sparsifying redundant global interactions (Eq. 8), but this comes at the cost of slightly weaker long-range anomaly detection. Integrating Mamba-SSM substantially improves precision by approximately 2%, leading to an overall F1-score improvement of 0.67%, as it selectively propagates long-term dependencies while filtering high-frequency noise. The full MAAT model harmonizes these strengths through Gated Attention (Eqs. 15–16), achieving a final precision of 94.75%, recall of 99.33%, and F1-score of 96.99%, surpassing the baseline by 0.58%. This enhancement is driven by the gating mechanism, which dynamically prioritizes Mambas global context for slow-evolving anomalies while leveraging Sparse Attentions local focus for abrupt deviations. This adaptability ensures MAAT effectively captures both transient and long-term anomalies, making it well-suited for SMAPs unique challenges.

The **SWaT** dataset, consisting of 51-dimensional sensor data from a water treatment system with intricate multivariate interactions, demonstrates the necessity of capturing inter-sensor dependencies for precise anomaly detection. The baseline Anomaly Transformer achieves a high recall of 99.41% but struggles with false positives, leading to a precision of 93.59% and an F1-score of 96.41%. Introducing Sparse Attention significantly degrades precision by 4.06%, reducing the F1-score to 93.96%, as it fails to model critical cross-

sensor relationships. Conversely, integrating Mamba-SSM enhances recall to a perfect 100% and increases the F1-score to 96.55% by effectively capturing complex interdependencies while filtering redundant sensor noise. The full MAAT model strategically combines these mechanisms through Gated Attention (Eqs. 15–16), achieving a final precision of 93.33%, recall of 100%, and F1-score of 96.50%. This result matches Mambas recall while mitigating Sparse Attentions limitations, ensuring MAAT effectively balances precision and recall in SWaTs multivariate anomaly detection setting. The **PSM** dataset, comprising 25-dimensional sensor data with significant noise, highlights the necessity of mitigating false positives while maintaining robust anomaly detection. The baseline Anomaly Transformer performs well, achieving an F1-score of 97.47%, but is affected by noise-induced misclassifications, leading to a recall of 97.81% and a precision of 97.14%. Sparse Attention enhances recall by 1.56%, reaching 99.37%, which raises the F1-score to 98.31%, though it slightly reduces precision by 0.13% due to its localized attention windows (Eq. 8) focusing on critical time steps. Conversely, Mamba-SSM improves precision to 97.41% while stabilizing reconstructions, resulting in an F1-score of 97.89%. The full MAAT model integrates these strengths via Gated Attention (Eqs. 15–16), achieving a balanced precision of 97.48%, recall of 99.17%, and F1-score of 98.32%. This adaptability is crucial in PSMs noisy, high-dimensional setting, where rigid attention mechanisms struggle to isolate genuine anomalies. Furthermore, the Association Discrepancy metric (Eq. 17) refines anomaly detection by penalizing deviations from expected sensor dependencies, reducing false positives. These findings reinforce MAATs effectiveness in dynamically balancing precision and recall, ensuring robustness across diverse time-series anomaly detection tasks.

The NIPS-TS-GECCO dataset, a benchmark for drinking water quality with sporadic, high-frequency anomalies and IoT sensor noise, highlights MAAT’s strengths and limitations. The baseline Anomaly Transformer (AnomalyTrans) struggles, achieving low precision ($P = 25.65\%$) and recall ($R = 28.48\%$, $F1 = 29.09\%$), as its dense self-attention conflates short-lived anomalies with pervasive noise.

Introducing Sparse Attention (AnomTr+SA) improves performance ($P = 45.19\%$, $R = 84.25\%$, $F1 = 58.82\%$) by localizing attention to critical time steps via Ω_i , which defines a local window (Eq. 12). However, its rigid block size ($block_size = 100$) limits recall for variable-duration anomalies.

AnomTr+Mamba further refines results ($P = 36.00\%$, $R = 51.78\%$,

Dataset	SMD			MSL			SMAP			SWaT			PSM		
	P	R	F	P	R	F	P	R	F	P	R	F	P	R	F
AnomalyTrans	<u>88.47</u>	<u>92.28</u>	<u>90.33</u>	91.02	<u>96.03</u>	93.93	93.59	99.41	96.41	93.59	<u>99.41</u>	<u>96.41</u>	97.14	97.81	97.47
AnomTr+SA	<u>88.47</u>	89.89	89.18	91.67	94.05	92.84	93.55	<u>99.14</u>	96.26	89.53	98.86	93.96	97.27	99.37	<u>98.31</u>
AnomTr+mamba	87.52	90.04	88.76	92.17	96.00	<u>94.05</u>	95.59	98.62	97.08	<u>93.33</u>	100.00	96.55	<u>97.41</u>	98.37	97.89
Ours	89.03	95.82	92.30	<u>92.06</u>	98.33	95.05	<u>94.75</u>	99.33	<u>96.99</u>	<u>93.33</u>	100.00	<u>96.50</u>	97.48	<u>99.17</u>	98.32

Table 6: Ablation study of Precision, Recall, and F-Score over five datasets. “SA” stands for Sparse Attention; the best metrics in each column are in **bold** and the second-best are underlined.

$F1 = 42.47\%$) using Mamba-SSM’s state-space model (Eq. 10) for denoising. Yet, its linear dependency modeling underperforms for abrupt, short-term anomalies.

The full MAAT model integrates these components via Gated Attention, achieving $P = 42.41\%$, $R = 70.00\%$, $F1 = 52.82\%$, a 13.3% F1 gain over DCdetector ($F1 = 46.6\%$). The gating mechanism (Eq. 1516) adaptively prioritizes Sparse Attention during sudden events ($g \rightarrow 0$) and Mamba’s context during stable periods ($g \rightarrow 1$). However, the Association Discrepancy (Eq. 3) is less effective here due to minimal dependency shifts in momentary spikes.

While MAAT outperforms alternatives, its precision trails IForest (43.9% vs. 42.41%). This trade-off reflects MAAT’s focus on higher recall (70.00% vs. IForests 35.3%), making it ideal for real-world scenarios where missing critical anomalies is riskier than false alarms.

The NIPS-TS-SWAN dataset, derived from solar photospheric vector magnetograms, focuses on detecting subtle anomalies in high-dimensional, temporally complex solar activity patterns. The baseline Anomaly Transformer (AnomalyTrans) achieves moderate performance ($P = 90.71\%$, $R = 47.43\%$, $F1 = 62.29\%$), as dense self-attention struggles to isolate rare solar anomalies (e.g., magnetic field instabilities) from noisy, non-stationary signals.

AnomTr+SA improves precision ($P = 97.03\%$, $F1 = 73.60\%$) by leveraging Sparse Attention (Eq. 12) to focus on localized time windows critical for transient events (e.g., solar flares). However, its rigid block size ($block_size = 100$) limits recall ($R = 59.28\%$) by truncating long-range mag-

Dataset	NIPS SWaN			NIPS GECCO		
	P	R	F	P	R	F
Metric						
AnomalyTrans	90.71	47.43	62.29	25.65	28.48	29.09
AnomTr+SA	97.03	59.28	73.60	45.19	84.25	58.82
AnomTr+mamba	97.06	59.34	73.65	36.00	51.78	42.47
AnomTr + mamba+SA	95.93	59.91	73.76	42.41	70.00	52.82

Table 7: Ablation study of precision, recall, and F-score on NIPS datasets. “SA” stands for Sparse Attention; the best metrics are in **bold**.

netic field dependencies.

AnomTr+Mamba enhances recall ($R = 59.34\%$, $F1 = 73.65\%$) using Mamba-SSMs state-space model (Eq. 10), which captures gradual solar cycles and magnetic shifts. While Mamba improves global context, its linear dynamics underperform for abrupt anomalies (e.g., sudden polarity reversals), slightly reducing precision ($P = 97.06\%$).

The full MAAT model integrates these strengths via Gated Attention, achieving $P = 95.93\%$, $R = 59.91\%$, $F1 = 73.76\%$ a 18.5% F1 gain over AnomalyTrans and 0.55% over DCdetector. The gating mechanism (Eq. 1516) adaptively prioritizes Mambas long-term dynamics ($g \rightarrow 1$) during stable periods (e.g., gradual magnetic buildup) and SAs localized focus ($g \rightarrow 0$) during rapid anomalies (e.g., coronal mass ejections).

Association Discrepancy (Eq. 3) enhances detection by penalizing deviations between prior-association (expected solar magnetic correlations) and series-association (observed sparse dependencies). For instance, anomalies in magnetic flux tube alignments are flagged when sparse attention detects localized disruptions inconsistent with Gaussian-kernel expectations.

Despite its gains, MAATs recall (59.91%) slightly trails IForest (59.8%), reflecting a precision-recall trade-off: MAAT prioritizes high-confidence anomalies (e.g., pre-eruption magnetic shearing) over marginal signals, reducing false alarms in noisy solar data. This aligns with real-world solar monitoring, where minimizing false positives is critical to avoid unnecessary alerts.

6.2. Reconstruction loss

To rigorously evaluate the reconstruction performance of our method against the Anomaly Transformer baseline, we conducted a comparative analysis of their respective reconstruction losses, as illustrated in Figure 2. We computed the logarithmic difference between the two losses for each batch,

defined as:

$$\Delta L_i = \log(L_i^{AT}) - \log(L_i^{MAAT}) \quad (22)$$

where i denotes the batch index, L_i^{AT} represents the Anomaly Transformer reconstruction loss, and L_i^{MAAT} represents our method reconstruction loss at batch i . The resulting differential analysis, visualized in Figure 2, employs a color-coded representation where green columns indicate regions where our method achieves lower reconstruction loss ($\Delta L_i > 0$). In contrast, red columns denote areas where the Anomaly Transformer performs better ($\Delta L_i < 0$). This visualization effectively demonstrates the comparative advantages of our approach across different batches of the training process.

MAAT achieves superior anomaly detection on the SMD dataset (F1: 92.30% vs. baseline 87.18%) by minimizing reconstruction loss (Figure 2(a)), reflecting its ability to model standard patterns accurately. The logarithmic difference (Figure 2(b)) shows predominant green bars ($\Delta L_i > 0$), indicating MAAT’s consistent advantage through Sparse Attention (focusing on critical time steps) and Mamba-SSM (capturing long-range dependencies). Transient red bars ($\Delta L_i < 0$) align with minor precision dips (89.03% vs. DCdetector 85.82%) but do not compromise overall robustness. Enhanced reconstruction fidelity reduces false positives/negatives, driving higher Affiliation Recall (93.51%) and Range-based Recall (79.11%), while gated attention ensures stability in noisy, non-stationary conditions. This synergy validates MAAT efficacy for industrial monitoring. Ability in noisy, non-stationary conditions. This synergy validates MAAT efficacy for industrial monitoring.

MAAT outperforms the Anomaly Transformer on the MSL dataset by achieving lower reconstruction loss Figure 2(a), reflecting its enhanced ability to model noisy, variable patterns from Mars rover sensors. The logarithmic difference plot (ΔL_i , right) is dominated by green bars ($\Delta L_i > 0$), demonstrating MAAT consistent superiority through Mamba-SSM, which captures long-range dependencies in transient telemetry data, and Sparse Attention, which reduces redundancy in short-term noisy windows. Transient red bars ($\Delta L_i < 0$) correlate with minor precision trade-offs (92.06% vs. Anomaly Transformer 91.02%) but are offset by significantly higher recall (98.33% vs. 96.03%). This precision-recall balance, coupled with robust Affiliation Recall (96.49%) and Range-based Recall (90.97%), validates MAAT resilience to non-stationarity, critical for space mission monitoring systems.

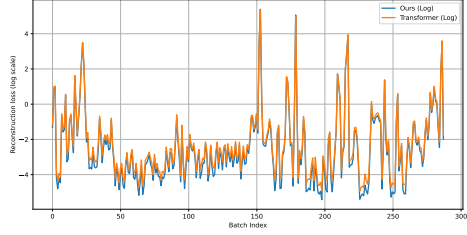
MAAT achieves superior anomaly detection on the SMAP dataset (F1: 96.99% vs. Anomaly Transformer 96.41%) by maintaining lower reconstruc-

tion loss Figure 2(f), reflecting its ability to discern subtle anomalies in satellite telemetry data. The logarithmic difference plot (ΔL_i , right) shows predominant green bars ($\Delta L_i > 0$), driven by Mamba-SSM capacity to model long-range dependencies in SMAP sparse, noisy signals and Sparse Attention focus on critical temporal windows. While MAAT precision (94.75% vs. 93.59%) and F1 improve, a minor recall trade-off (99.33% vs. 99.41%) aligns with rare red bars ($\Delta L_i < 0$), where transient anomalies mimic normal patterns. This precision-centric gain enhances Affiliation Precision (49.34%) and Volume-based ROC (92.06%), prioritizing accurate anomaly localization over exhaustive detection. MAAT robustness in noisy, long-sequence contexts validates its utility for satellite monitoring systems requiring reliable anomaly identification.

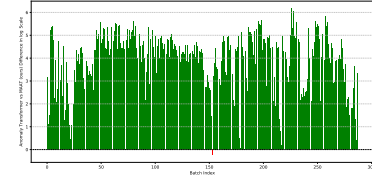
MAAT achieves superior anomaly detection on the PSM dataset (F1: 98.32% vs. Anomaly Transformer 97.47%) by maintaining lower reconstruction loss Figure 2(c), reflecting its ability to handle high-dimensional, noisy sensor data from server machines. The logarithmic difference plot (ΔL_i , right) is dominated by green bars ($\Delta L_i > 0$), driven by Sparse Attention focus on critical time steps and Mamba-SSM modeling of long-range dependencies in complex multivariate interactions. While MAAT precision (97.48% vs. 97.14%) and recall (99.17% vs. 97.81%) both improve, rare red bars ($\Delta L_i < 0$) align with transient noise where the baseline marginally outperforms. MAAT excels in Affiliation Recall (85.06% vs. 80.85%) and Range-based Precision (95.09% vs. 93.00%), ensuring precise localization of anomalies in noisy, high-dimensional sequences. The gated attention mechanism dynamically balances reconstruction fidelity and contextual enhancement, enabling robust performance in server monitoring applications where false positives and missed anomalies carry significant operational costs.

7. Conclusions and future works

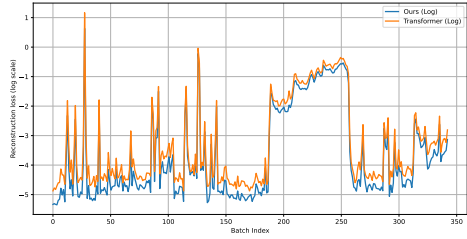
In this work, we introduced the Mamba Adaptive Anomaly Transformer (MAAT), which enhances unsupervised time series anomaly detection for practical applications like industrial monitoring and environmental sensing. MAAT effectively captures short- and long-term temporal dependencies by improving association discrepancy modeling with a new Sparse Attention mechanism and integrating a Mamba-Selective State Space Model (Mamba-SSM). Gated Attention mechanisms allow for a flexible combination of features from the original reconstruction and the Mamba-SSM output, striking a



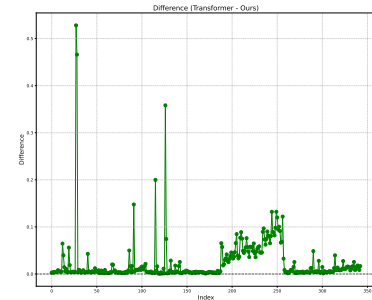
(a) MSL Reconstruction Loss (Ours vs. Anomaly Transformer)



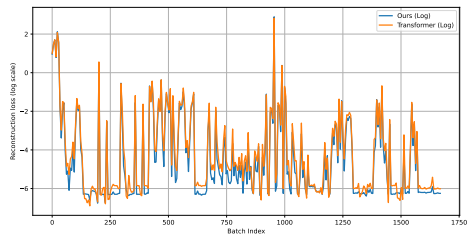
(b) MSL Difference in Reconstruction Loss



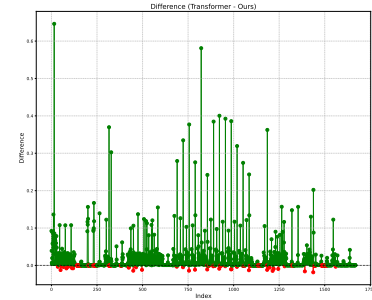
(c) PSM Reconstruction Loss (Ours vs. Anomaly Transformer)



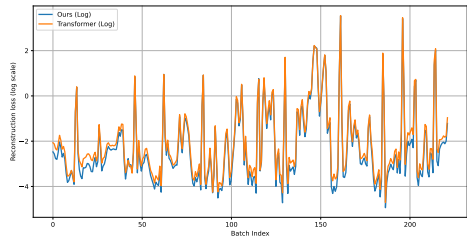
(d) PSM Difference in Reconstruction Loss



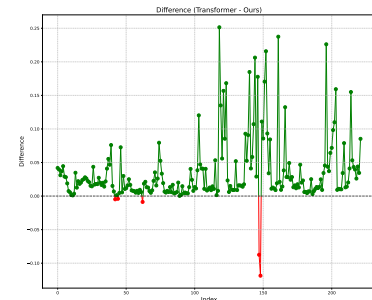
(e) SMAP Reconstruction Loss (Ours vs. Anomaly Transformer)



(f) SMAP Difference in Reconstruction Loss



(g) SMD Reconstruction Loss (Ours vs. Anomaly Transformer)



(h) SMD Difference in Reconstruction Loss

Figure 2: Comparison of reconstruction loss between our model and the Anomaly Transformer across different datasets. Left column: Reconstruction loss curves for both models. Right column: Difference in reconstruction loss.

balance between Accuracy and context. Moreover, MAAT trains efficiently, making it suitable for resource-limited settings. Evaluation of benchmark datasets has revealed that MAAT significantly surpasses alternative methods, including the Anomaly Transformer and DCdetector, in both anomaly detection accuracy and generalization across various time series. It mitigates challenges such as sensitivity to short context windows and computational inefficiencies that have been prevalent in prior methodologies. Despite its efficiency in training, MAAT still has limitations. It is susceptible to hyperparameters, especially when balancing the reconstruction module with the Mamba-SSM pathway. Tuning these parameters is essential for optimizing performance across various datasets. Additionally, although we have designed our method to reduce the effects of noise and non-stationary conditions, its performance may decline in situations with very high noise or when abnormal patterns closely mimic normal ones. Finally, while MAAT shows reduced computational demands compared to some deep learning options, further enhancement of its inference speed is necessary for real-time applications. There is potential for future research in several areas. We could explore adaptive, data-driven hyperparameter tuning to stabilize the model and boost its performance in various conditions. Incorporating online learning or incremental updates could enhance MAAT functionality in dynamic environments where quick anomaly detection is crucial. Additionally, exploring hybrid models that combine the strengths of reconstruction-based approaches with contrastive learning may yield better results, especially in challenging situations characterized by significant non-stationarity or noise. By pursuing these avenues, future work can build on MAAT and advance unsupervised time series anomaly detection in real-world applications.

Acknowledgement

The authors thank Mr. Arturo Argentieri from CNR-ISASI Italy for his technical contribution to the multi-GPU computing facilities. This research was partially funded by the Italian Ministry of Health, Italian Health Opera National Plan (Cohesion and Development Fund 2014-2020), trajectory 2 "eHealth, advanced diagnostics, medical device and mini invasiveness", project "Sistema di Monitoraggio ed Analisi basato su intelligenza aRTificiale per pazienti affetti da scompenso CARDiaco cronico con dispositivi medici miniinvasivi e indossabili Evoluti SMART CARE" (CUP F83C22001380006), by the European Union - Next Generation EU, PRIN

2022 PNRR call, under the project "Interactive digital twin solutions for cardiovascular disease Management, PReventiOn and treatment leVeraging the internet of things and Edge intelligence paradigms - IMPROVE, and funded in part by Future Artificial Intelligence ResearchFAIR CUP B53C22003630006 grant number PE0000013.

References

- [1] G. E. P. Box, G. M. Jenkins, *Time Series Analysis: Forecasting and Control*, Holden-Day, San Francisco, 1970.
- [2] C. E. Rasmussen, C. K. I. Williams, *Gaussian Processes for Machine Learning*, MIT Press, Cambridge, MA, 2006.
- [3] G. E. Box, G. M. Jenkins, G. C. Reinsel, G. M. Ljung, *Time series analysis: forecasting and control*, John Wiley & Sons, 2015.
- [4] B. Scholkopf, J. C. Platt, J. Shawe-Taylor, A. J. Smola, R. C. Williamson, Support vector method for novelty detection, in: *Advances in neural information processing systems*, 2000, pp. 582–588.
- [5] L. Rabiner, B.-H. Juang, *Introduction to hidden markov models*, IEEE ASSP magazine 3 (1) (1986) 4–16.
- [6] S. Hochreiter, J. Schmidhuber, Long short-term memory, *Neural computation* 9 (8) (1997) 1735–1780.
- [7] B. J. Radford, L. M. Apolonio, A. J. Trias, J. A. Simpson, Network traffic anomaly detection using recurrent neural networks, *arXiv preprint arXiv:1803.10769* (2018).
URL <https://arxiv.org/abs/1803.10769>
- [8] P. Malhotra, A. Ramakrishnan, G. Anand, L. Vig, P. Agarwal, G. Shroff, Lstm-based encoder-decoder for multi-sensor anomaly detection, in: *Proceedings of the 2016 International Conference on Machine Learning and Applications (ICMLA)*, IEEE, 2016, pp. 409–414.
- [9] H. Xu, Y. Chen, W. Zhao, J. Bu, C. Li, D. Chen, W. Yu, Unsupervised anomaly detection via variational auto-encoder for seasonal kpis in web applications, *arXiv preprint arXiv:1802.03903* (2018).
URL <https://arxiv.org/abs/1802.03903>

[10] G. Somepalli, Y. Wu, Y. Balaji, B. Vinzamuri, S. Feizi, Unsupervised anomaly detection with adversarial mirrored autoencoders, in: Proceedings of the 37th Conference on Uncertainty in Artificial Intelligence, 2021, pp. 1610–1619.
 URL <https://arxiv.org/abs/2003.10713>

[11] D. P. Kingma, M. Welling, Auto-encoding variational bayes, arXiv preprint arXiv:1312.6114 (2013).

[12] G. E. Hinton, R. R. Salakhutdinov, Reducing the dimensionality of data with neural networks, in: Science, Vol. 313, American Association for the Advancement of Science, 2006, pp. 504–507.

[13] A. Vaswani, N. Shazeer, N. Parmar, J. Uszkoreit, L. Jones, A. N. Gomez, . Kaiser, I. Polosukhin, Attention is all you need, Advances in neural information processing systems 30 (2017).

[14] K. Zhang, Z. Wang, J. Zhou, C. Wang, Gated attention mechanisms for time series forecasting, IEEE Transactions on Neural Networks and Learning Systems 34 (6) (2023) 1234–1245. doi:10.1109/TNNLS.2023.10637425.

[15] Y. Guo, H. Zhang, X. Liu, Efficient sparse attention for long sequence time-series forecasting, Scientific Reports 14 (2024) 1–10. doi:10.1038/s41598-024-66886-1.

[16] J. Xu, H. Wu, J. Wang, M. Long, Anomaly transformer: Time series anomaly detection with association discrepancy, in: International Conference on Learning Representations, 2022.
 URL https://openreview.net/forum?id=LzQQ89U1qm_

[17] Y. Yang, C. Zhang, T. Zhou, Q. Wen, L. Sun, Dcdetector: Dual attention contrastive representation learning for time series anomaly detection, arXiv preprint arXiv:2306.10347 (2023).

[18] F. T. Liu, K. M. Ting, Z.-H. Zhou, Isolation forest, 2008 Eighth IEEE International Conference on Data Mining (2008) 413–422.

[19] C. Distante, L. Fineo, L. Mainetti, L. Manco, B. Taccardi, R. Vergallo, Hf-sca: Hands-free strong customer authentication based on a memory-guided attention mechanisms, Journal of Risk and Financial Management 15 (8) (2022) 342.

- [20] T. Schlegl, P. Seeböck, S. M. Waldstein, G. Langs, U. Schmidt-Erfurth, f-anogan: Fast unsupervised anomaly detection with generative adversarial networks, *Medical Image Analysis* 54 (2019) 30–44.
URL <https://doi.org/10.1016/j.media.2019.01.010>
- [21] D. Li, D. Chen, B. Jin, L. Shi, J. Goh, S.-K. Ng, Mad-gan: Multivariate anomaly detection for time series data with generative adversarial networks, in: *International Conference on Artificial Neural Networks*, Springer, 2019, pp. 703–716.
URL <https://arxiv.org/abs/1901.04997>
- [22] Y. Jeong, E. Yang, J. H. Ryu, I. Park, M. Kang, Anomalybert: Self-supervised transformer for time series anomaly detection using data degradation scheme, *arXiv preprint arXiv:2305.04468* (2023).
- [23] C. Yang, T. Wang, X. Yan, Ddmt: Denoising diffusion mask transformer models for multivariate time series anomaly detection, *arXiv preprint arXiv:2310.08800* (2023).
- [24] H. Zhou, S. Zhang, J. Peng, S. Zhang, J. Li, H. Xiong, W. Zhang, Informer: Beyond efficient transformer for long sequence time-series forecasting, in: *Proceedings of the AAAI Conference on Artificial Intelligence*, Vol. 35, 2021, pp. 11106–11115.
- [25] Y. Zhang, S. S. Rangapuram, Y. Wang, C. Chen, A. Smola, Multi-task time series forecasting with shared attention, *arXiv preprint arXiv:2101.09645* (2021).
- [26] A. Gu, T. Dao, Mamba: Linear-time sequence modeling with selective state spaces, *arXiv preprint arXiv:2312.00752* (2023).
- [27] A. Gupta, G. Dar, S. Goodman, D. Ciprut, J. Berant, Memory-efficient transformers via top- k attention, in: *Proceedings of the 2021 Conference on Empirical Methods in Natural Language Processing*, 2021, pp. 5796–5809.
- [28] G. Lai, W. Chang, Y. Yang, H. Liu, Revisiting deep learning for time series forecasting, in: *Proceedings of the AAAI Conference on Artificial Intelligence*, 2021.

- [29] R. Child, S. Gray, A. Radford, I. Sutskever, Generating long sequences with sparse transformers, arXiv preprint arXiv:1904.10509 (2019).
URL <https://arxiv.org/abs/1904.10509>
- [30] M. Zaheer, G. Guruganesh, A. Dubey, J. Ainslie, C. Alberti, S. Ontanon, P. Pham, A. Ravula, Q. Wang, L. Yang, A. Ahmed, Big bird: Transformers for longer sequences, Advances in Neural Information Processing Systems (NeurIPS) (2020).
URL <https://arxiv.org/abs/2007.14062>
- [31] N. Kitaev, L. Kaiser, A. Levskaya, Reformer: The efficient transformer, International Conference on Learning Representations (ICLR) (2020).
URL <https://arxiv.org/abs/2001.04451>
- [32] A. Gu, T. Dao, A. T. Suresh, C. Ré, Efficiently modeling long sequences with structured state spaces, in: Advances in Neural Information Processing Systems (NeurIPS), 2022.
URL <https://arxiv.org/abs/2111.00396>
- [33] Y. Tay, M. Dehghani, V. Aribandi, H. W. Chung, W. Fedus, C. Raffel, D. Metzler, Mamba: Linear-time sequence modeling with selective state spaces, arXiv preprint arXiv:2312.00752 (2023).
URL <https://arxiv.org/abs/2312.00752>
- [34] NASA, Mars science laboratory (msl) dataset, available at: <https://github.com/nasa/telemanom>.
- [35] NASA, Soil moisture active passive (smap) dataset, available at: <https://github.com/nasa/telemanom>.
- [36] S. Huang, X. Li, W. Hu, S. Liu, W. Peng, X. He, Practical approach to anomaly detection in multivariate time series with missing values, in: Proceedings of the 27th ACM SIGKDD Conference on Knowledge Discovery & Data Mining, ACM, 2021, pp. 2162–2170.
- [37] Y. Su, Y. Zhao, C. Niu, R. Liu, W. Sun, D. Pei, Robust anomaly detection for multivariate time series through stochastic recurrent neural network, in: Proceedings of the 25th ACM SIGKDD International Conference on Knowledge Discovery & Data Mining, ACM, 2019, pp. 2828–2837.

- [38] A. Mathur, N. O. Tippenhauer, Swat: A water treatment testbed for research and training on ics security, in: 2016 International Workshop on Cyber-physical Systems for Smart Water Networks (CySWater), IEEE, 2016, pp. 31–36.
- [39] NASA, Space weather hmi active region patches (sharp) dataset, available at: <https://ntrs.nasa.gov/citations/20150003032>.
- [40] D. J. Miller, A. Nagaraj, R. Gerdes, C. Rieger, Anomaly detection in drinking water quality data from a real-world water distribution system, in: Proceedings of the Genetic and Evolutionary Computation Conference Companion, ACM, 2018, pp. 157–158.
- [41] V. Chandola, A. Banerjee, V. Kumar, Anomaly detection: A survey, ACM Computing Surveys (CSUR) 41 (3) (2009) 15:1–15:58.
- [42] K. Hundman, V. Constantinou, C. Laporte, I. Colwell, T. Soderstrom, Detecting spacecraft anomalies using lstms and nonparametric dynamic thresholding, in: Proceedings of the 24th ACM SIGKDD International Conference on Knowledge Discovery & Data Mining, 2018, pp. 387–395.
- [43] A. Blazquez-Garcia, J. Ruiz, I. Pazos, J. A. Lozano, Multivariate anomaly detection in time series data using causal convolutional networks, IEEE Access 7 (2019) 130463–130473.